JGR Atmospheres

RESEARCH ARTICLE
10.1029/2021JD036294

Evaluation of Eddy Covariance Footprint Models Through the Artificial Line Source Emission of Methane

Shuo Liu[1,2], Gang Liu[3], Mi Zhang[4], Yufang Sun[3], Shuangxi Fang[1], Xiaojie Zhen[5], and Zhaozhong Feng[4]

[1]Zhejiang Carbon Neutral Innovation Institute, Zhejiang University of Technology, Hangzhou, China, [2]State Key Laboratory of Urban and Regional Ecology, Research Center for Eco-Environmental Sciences, Chinese Academy of Sciences, Beijing, China, [3]State Key Laboratory of Soil and Sustainable Agriculture, Institute of Soil Science, Chinese Academy of Sciences, Nanjing, China, [4]Key Laboratory of Agrometeorology of Jiangsu Province, School of Applied Meteorology, Nanjing University of Information Science & Technology, Nanjing, China, [5]Jiangsu Tynoo Corporation, Wuxi, China

Abstract This paper evaluates the performance of footprint models through a line source (LS) system releasing methane (CH_4) measured by an eddy covariance (EC) system in a rice-wheat rotation agro-ecosystem. Two footprint models namely Kormann and Meixner (KM) and Flux Footprint Prediction (FFP), are used. The "line source width (LW)" was introduced, which could highly impact the model estimation, leading to an error of ~500% for the FFP and ~200% for the KM. The surface roughness length (z_0) also affects the FFP estimation, which is much weaker than the effect of LW with a 15% error. An overestimation of 217.8% is observed when the LS is close to the EC system, which reduces to 12.2% when the source stays distant. The analysis of different experimental configurations illustrated that the estimated emission calculated based on footprint model improves with increasing emission height, averaging period, and emission rate. The most accurate estimations are achieved by the configurations of canopy level (CL; 5.5% overestimation), 15 min averaging period (1% underestimation), and moderate emission (ME; 1.9% underestimation), respectively. For KM, the CL-ME-30 min setup leads to the best performance, while SL (soil level)-ME-15 min is the best configuration for the FFP estimation. A multivariate regression model is proposed to provide preliminary guidance for the footprint model application. The designed LS system is valuable for validating the performance of flux measurements in the specific ecosystems (e.g., grassland, sand land, and forest) as well as other greenhouse gases (e.g., N_2O and NH_3).

Plain Language Summary A line-source system, which can automatically simulate methane emission in the paddy fields, was designed to evaluate the performance of eddy covariance footprint models. Different emission heights, emission rates, and source distances were conducted. The result suggested that the outputs of the footprint model improved with increasing emission height and emission rate. The most accurate model estimation was found at the canopy height and the moderate emission. Finally, the range of estimation errors was calculated quantitatively, and a multivariate regression model was proposed to evaluate footprint model performance. The designed line-source system is also available for validation in other ecosystems, such as grassland and sand land.

Key Points:

- Footprint model estimation improves with increasing source emission height, averaging period, and emission rate
- Source width and emission distance can significantly affect the model performance
- The most accurate estimations are achieved at the canopy level, 15 min averaging period, and moderate emission

Supporting Information:

Supporting Information may be found in the online version of this article.

Correspondence to:

X. Zhen and Z. Feng,
zhenxj@technosolutions.cn;
zhaozhong.feng@nuist.edu.cn

Citation:

Liu, S., Liu, G., Zhang, M., Sun, Y., Fang, S., Zhen, X., & Feng, Z. (2022). Evaluation of eddy covariance footprint models through the artificial line source emission of methane. *Journal of Geophysical Research: Atmospheres*, *127*, e2021JD036294. https://doi.org/10.1029/2021JD036294

Received 3 DEC 2021
Accepted 2 AUG 2022

1. Introduction

The eddy covariance (EC) methodology has gained significant attention over the past two decades in investigating the scalar exchange between the atmosphere and the biosphere (Foken et al., 2012). The EC methodology can detect relevant ecosystem fluxes by means of high-frequency measurements of three-dimensional (3D) wind speed, wind direction, air temperature, trace gas concentration, and many other variables to capture turbulent motions (Aubinet et al., 2000). The flux measured by EC mainly represents an integrated signal from all sources and sinks within the flux footprint from the underlying surface of source regions in a specific ecosystem. The contribution of flux sources/sinks may not be the same in different locations of the surface boundary layer if the atmospheric and surface conditions are not identical (Heidbach et al., 2017; Schmid, 2002). It is crucial to define the relationship between turbulent fluxes, corresponding surface layers to evaluate the effective flux source area of each flux measurement (Gockede et al., 2004; Horst & Weil, 1995; Rebmann et al., 2012). Hence, the "footprint" notion was established by micrometeorologists, and different footprint models of various complexity were developed to describe the mathematical relationship between the effective source region and the measured fluxes

for a quantitative calculation addressing the above issue (Rannik et al., 2012; Schuepp et al., 1990). The computation of footprint is essential to acquire more information about the contribution of different areas within the source regions (Chasmer et al., 2011; Heidbach et al., 2017; Van de Boer et al., 2013; Wagle et al., 2020), which allows for the correct interpretation of EC measurements.

There are various footprint models proposed in the literature (Gockede et al., 2005; Leclerc & Foken, 2014; Rannik et al., 2012; Schmid, 2002). Among them, three main categories are commonly used: (a) analytical or analytical-like models (e.g., Kljun et al., 2015; Kormann & Meixner, 2001), (b) Lagrangian stochastic particle dispersion models (e.g., Flesch et al., 1995; Kljun et al., 2002), and (c) large eddy simulation (e.g., Leclerc et al., 1997; Steinfeld et al., 2008). These models often use commonly available parameters and quantities, which can be computed and derived using EC measurements, such as wind direction, friction velocity (u_*), roughness length (z_0), and standard deviation of lateral wind component (σ_v) (Van de Boer et al., 2013). Nevertheless, with the application and development of models, some of the questions remain unsolved, for example, whether the footprint model can accurately estimate the contribution area (Leclerc & Foken, 2014). The source areas measured by EC in a specific ecosystem can be largely dependent on the measurement height. The existing models assume the sources are at the soil surface level or below the displacement height; hence, the influence of the release height remains unclear (Dumortier et al., 2019). Furthermore, the responses of different scalar fluxes or meteorological components to the footprint models are still unsolved (Foken & Leclerc, 2004).

Until now, only a few experiments and simulations have been performed to evaluate the footprint models and the issues discussed above (Foken & Leclerc, 2004). The existing efforts used approaches mainly based on natural tracers (Arriga et al., 2017; Gockede et al., 2005; Marcolla & Cescatti, 2005; Nicolini et al., 2017; Reth et al., 2005; Van de Boer et al., 2013) or artificial tracers with different artifactitious sources (Arriga et al., 2017; Dumortier et al., 2019; Finn et al., 1996; Heidbach et al., 2017; Leclerc et al., 2003; Mauder & Foken, 2011). Experimenting with natural tracers is inexpensive and easy to perform; however, it relies heavily on the corresponding surface of the experiment. For example, Gockede et al. (2004, 2005) evaluated different footprint models using the heterogeneity of the surface to evaluate the model performance on varying land-cover types. Van de Boer et al. (2013) evaluated analytical footprint models using natural tracers from different land-use types. As a result, they found an overestimation of the peak contribution distance of the models. For artificial tracer experiments, the validation could specifically or flexibly be designed. However, Artificial tracer experiments, are commonly more complex and expensive than natural tracer-based experiments. Reth et al. (2005) utilized the soil chamber approach and measured the EC flux to validate the footprint models. For the same goal, Leclerc et al. (2003) used sulfur hexafluoride as an artificial tracer. Heidbach et al. (2017) introduced another artificial tracer (a single point-source) to assess the performance of footprint models. The results revealed that most footprint models overestimate the peak contribution distance when point sources were close to the EC system, and changes in roughness length could affect model outputs. Arriga et al. (2017) cut vegetation successively over the experiment period, which illustrated the strong influence of surface roughness on the footprint models, indicating how crucial the further experiments are for improving the footprint models. Coates et al. (2017) designed eight-fixed artificial point sources and configured two release distances between those sources and the EC system to evaluate the accuracy of model estimation, which revealed the overestimation of the estimated emission calculated based on footprint model when the sources were in close distance. Dumortier et al. (2019) used an artificial point source to evaluate the application of different footprint models, the result of which suggested that the flux calculation approaches could highly affect the footprint model performance and performed well with the elevated release. As a result, the study emphasized the additional manipulative experiments on the influence of release height and distance (Dumortier et al., 2019).

In general, measurement height, surface roughness, and atmospheric stability are three main factors affecting the footprint (Leclerc & Thurtell, 1990). With increased measurement height or decreased roughness, upwind distance of peak contribution increased, while magnitude of the peak contribution decreased, and the upwind distance covered by the station and the zone of "no contribution" increased. Hence, both sufficient fetch and undisturbed area around the instrument are very important for proper footprint at a given measurement height and any roughness (Burba, 2001). Besides, changes in atmospheric stability can expand the footprint several times. Flux data at very stable conditions or very unstable conditions may need to be corrected or discarded because of the insufficient fetch or a large portion of the flux comes from an area very close to the instrument (Leclerc & Thurtell, 1990). For the evolution of models to continue, adequate experimental validation and

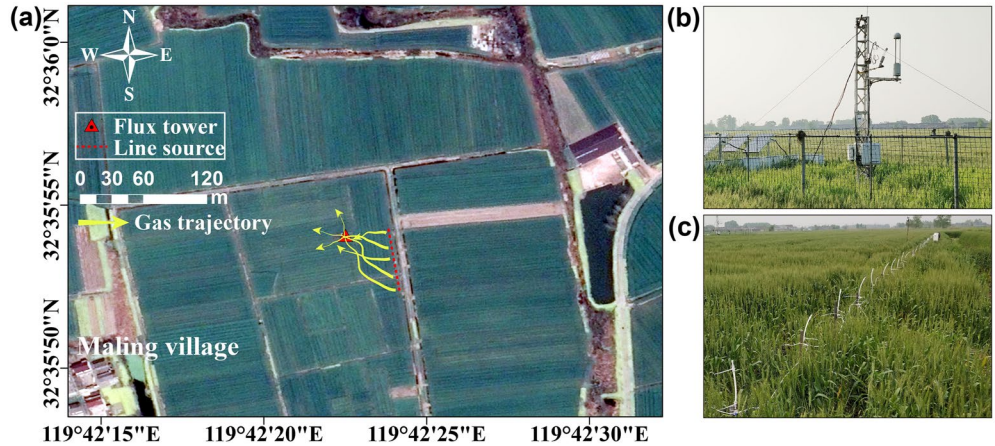

Figure 1. (a) The geographical location of flux tower and line source; (b) the photos of the eddy covariance system; (c) the line source device used in experiments. The arrowed yellow curves in (a) illustrate the imaginary transport pathways of the released CH_4 gases. The remote sensing image layer was downloaded from © Google Earth.

evaluation methods are crucial. However, due to the lack of validation data in the current literature, it is challenging to improve the footprint models; hence, the accuracy and applicability of the footprint models have remained unclear. Thus, more comprehensive and well-designed experiments are required to provide more significant references (Arriga et al., 2017; Dumortier et al., 2019).

According to the above-given efforts, the experiments should ideally simulate a real source-emission scenario in nature with an artificial tracer, and various source-emission setups should be established. In this study, we designed a line source (LS) device and an automatic emission control system measuring the artificially emitted methane (CH_4) by the EC system since the CH_4 signals from the LS could be better captured by the EC compared to a point source. To accurately simulate the real-emission process of CH_4 in the paddy field, the CH_4 sources were not only metered released, but also calibrated using natural emission values similar to paddy field. Besides, different experimental setups, that is, emission height, rate, and distance between the source and the EC system, were implemented. No such setups have been comprehensively applied to study the knowledge gaps discussed above. Hence, our study aims at (a) comparing the performance of footprint models in different experimental setting; (b) investigating the influence of potential causes that affect the model estimation; and (c) providing appropriate suggestions for the modification of the model application, to improve the application of footprint models.

2. Methodology

2.1. Flux Site and Instruments

The experiments were performed at a site located in Xiaoji Town, Jiangdu County, Jiangsu Province, China (32°35′54″N, 119°42′23″E, 5 m a.s.l) (Figure 1). The site location had two harvests, winter wheat and summer rice in rotation each year, under a sub-tropical maritime climate. During the experimental period (from 24 March to 28 April 2020), the site was planted with winter wheat (~300 × 300 m^2), which emitted near zero methane from the jointing stage to the grain filling stage. The average daily air temperature was 13.7°C, the accumulated precipitation was 146.8 mm, and the mean daytime (06:00–18:00, local time) vapor pressure deficit (VPD) was 0.1 kPa during the experiment period. Maling Village was approximately 250 m away from the southwest and had a population of ~500 people.

The flux observation tower of the EC system was erected alongside the downwind position of the predominant wind direction in this region (Figure 1). The EC system was installed at 3 m above ground level, including a 3D wind speed, sonic anemometer (CSAT3B, Campbell Scientific, Inc., Logan, UT, USA, hereinafter referred to as CSI), an open-path CO_2/H_2O gas analyzer (LI-7500RS, LI-COR, Inc., Lincoln, NE, USA), an open-path CH_4 gas analyzer (LI-7700, LI-COR, Inc., Lincoln, NE, USA), a temperature and humidity sensor (HMP155A, Vaisala, Inc., HKI, Finland), and a rain gauge (TYJ-2, Jiangsu Tynoo Corp., Wuxi, JS, China). The EC system was

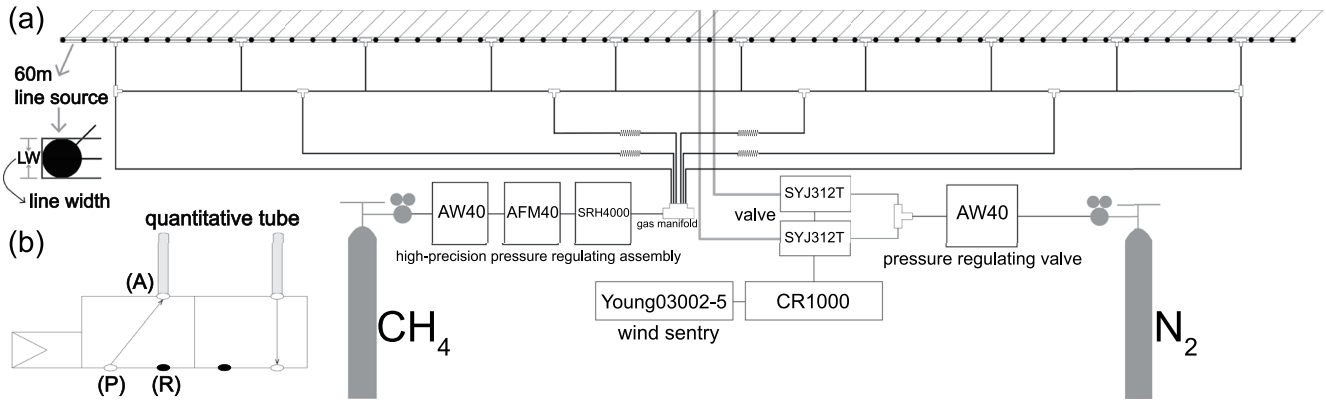

Figure 2. (a) The schematic of the line source system; (b) the release process of the source.

installed toward the predominant wind direction (120°). The 3D wind, sonic temperature, CO_2/CH_4/H_2O density, and air pressure were measured at 10 Hz in the 3D space. Air temperature and relative humidity were measured at an interval of 5 seconds. A data logger (CR6, CSI) collected all the data.

2.2. Experimental Setup

2.2.1. Line Source System

The point source was commonly used for tracer experiments (Coates et al., 2017; Dumortier et al., 2019; Heidbach et al., 2017), which was not typical for the LS (Arriga et al., 2017). A LS was commonly simulated by equally-spaced multiple point sources, which were much more complex than the single point sources due to uniformity and consistency of multiple point emissions. However, a relatively stable wind direction was essential for the validation experiments adopting point sources in field, due to determining whether the EC system could continuously and effectively measure the release source, thereby obtaining reliable experimental data. The EC system could not adequately measure the point source emissions, because the rapidly changing turbulence and the small point area. In contrast, a LS emission in the upwind of the EC system was more feasible.

Figure S1 in Supporting Information S1 shows the LS emission system designed in this study. The length of the LS was 60 m, and was placed along the north-south axis. The prevailing wind direction was 120° clockwise from North, and the LS covered the EC system from 90 to 150°. The EC systems was 35m from the north point of the LS to the flux tower (the horizontal distance), and 69.5 m from the south point of the LS to the flux tower (the maximum difference). In order to ensure the accuracy of the experimental measurement, the LS needs to be placed in the best source area under the EC measurement. Hence, before the experiment, we applied the footprint model to find the source distribution (probable peak contribution distance) when the environmental conditions were same to our experiment (e.g., wind directions). The distance between the LS and the flux tower was determined based on the peak contribution distance of the upwind footprint, using EC measurement data before the experiment.

2.2.2. Gas Pipelines

There were two separate pipelines supplying high purity CH_4 (P_C) and high purity nitrogen -N_2- (P_N). The tubes of P_C and P_N were made of polyurethane with an external and internal diameter of 4 and 2.5 mm, respectively. Figure 2 illustrates the schematic of the LS system. The 60 outlets of P_C were equally distributed with one outlet per meter. A balanced gas pipeline network was designed to ensure equal pressure of CH_4 at each outlet (Figure 2a). First, a gas manifold with a large diameter distributed the CH_4 to six tributaries through six tubes (6 mm/4 mm) of the same length. Then, the gas was distributed by the T-junctions to ensure equal gas pressure at each outlet. The outlets consisted of a pneumatic control valve (SYJA324) and a quantitative tube (Qt) (Figure 2b). The Qt was closed at one end and connected to the (A) port of an SYJA324 at the other end. The Qt was made of polyurethane with an external and internal diameter of 8 and 5 mm. Different length of Qt was designed, which aimed to accurately store gas and control the emission rate from each outlet by its length. CH_4 was connected to the (P) port of an SYJA324. N_2, on the other hand, was connected to the pneumatic port. Hence,

CH_4 could be uniformly emitted throughout the entire LS with the same gas pressure and the same amount of gas in each Qt.

N_2 was used as the pneumatic source of the valve (SYJA324) (see Sec 2.2.3) since CH_4 was flammable. CH_4 and N_2 were stored in cylinders (10 MPa, 8 L, containing 99.995% pure CH_4 or N_2), which could nearly supply 800 L of gas. The output pressures of CH_4 and N_2 at the cylinder were controlled by a 0.22–0.25 MPa pressure reducing valve. A high-precision pressure regulating assembly (AW40, AFM40, and SRH4000, SMC) was installed to stabilize the output pressure between 0.18 and 0.2 MPa in P_C. The gas pressure in P_N, however, was kept at 0.22 MPa by using a pressure regulating valve (AW40, SMC). The pressure error was less than 1%.

2.2.3. Control System

The control system was an instrumental assembly, which controlled the automatic inflation/exhaust process. It consisted of a data logger (CR1000, CSI), a 16-channel AC/DC relay controller (SDM-CD16AC, CSI), an R. M. Young wind sentry set (03002-5), a 12 V power supply with a charging regulator (PS100, CSI), an electromagnetic valve (12V, SYJ312T, SMC), and solar panels to power the system. Based on the SDM-CD16AC, the gas release could be controlled either automatically by the CR1000's program or manually by a toggle switch.

Figure 2b shows the release action with three steps: (a) when the 5 min average wind direction was between 90° and 150°, the system was turned on, and the two valves (SYJ312T, SMC) inflated/exhausted N_2 into P_N; (b) when N_2 was exhausted from P_N, the Qt was filled with CH_4 from (P) port to (A) port; (c) when N_2 was filled into P_N from the pneumatic port, CH_4 was released from Qt and the (R) port. The emission period was set to 20 s. The time required to exhaust CH_4 was 7 s, and the charging process was determined as 13 s. If the wind direction was not satisfied, CH_4 release had stopped immediately. The wind speed, wind direction, release time, and release counts were recorded every 5 min. The data were used to compute total emission and to filter the unreliable release period.

2.2.4. Various Setup

Different experimental setups were constructed to evaluate the footprint model performance in terms of source emission rates, emission heights, and emission distances. Each setup adopted different levels of experiment configurations, the detailed schematic diagram about the different experiment configurations could be seen in Figure S2 in Supporting Information S1.

- The release outlets were set to two different heights, 10 and 60 cm above the soil surface, representing soil level (SL) and canopy level (CL).
- Three different emission rates were designed, that is, low emission (LE), moderate emission (ME), and high emission (HE). Based on the pressure in the tube (0.19 MP), the one-time Qt emissions of LE, ME, and HE were 4.48, 8.21, and 12.68 (standard mL CH_4/20s), respectively.
- The entire LS was segmented into two parts to represent different distances according to the predominant wind direction (120°). The first part of the LS (0–20 m) was close to the EC system (CLS). In other words, it extended 20 m from the north point of the LS, while the other parts of the LS (20–60 m) were far away from the EC system (ALS), that is, from 20 m to the south point of the LS.

Almost all combined configurations were implemented to evaluate the response of the EC system and the footprint models, except the CL with 340 mm Qt, due to the rainy season and the ongoing wheat harvest at the site.

2.3. Flux Calculation

The raw EC data (10 Hz) were processed using EddyPro software (version 7.0.4, LI-COR Biosciences, Lincoln, NE, USA), following the standard procedures for EC measurements. Overall, the averaged fluxes were calculated following the procedures including diagnostic flags filtering and de-spiking, time delay removal (Foken et al., 2012; Horst & Lenschow, 2009), tilt correction (double rotation, Tanner & Thurtell, 1969), SND (Schotanus, Nieuwstadt, and Debruin., 1983, SND) correction, frequency loss corrections (Foken et al., 2012; Horst & Lenschow, 2009; Kaimal et al., 1989; Moncrieff et al., 1997; Moore, 1986; Van Dijk, 2002), WPL (Webb et al., 1980, WPL) correction and spectroscopic corrections (McDermitt et al., 2011), and quality control (QC) (Campbell Scientific Inc., 2017; Foken et al., 2012). Different averaging periods, that is, 5, 15, and 30 min, were utilized to evaluate the effect of the flux averaging period on the model performance. Sun et al. (2006)

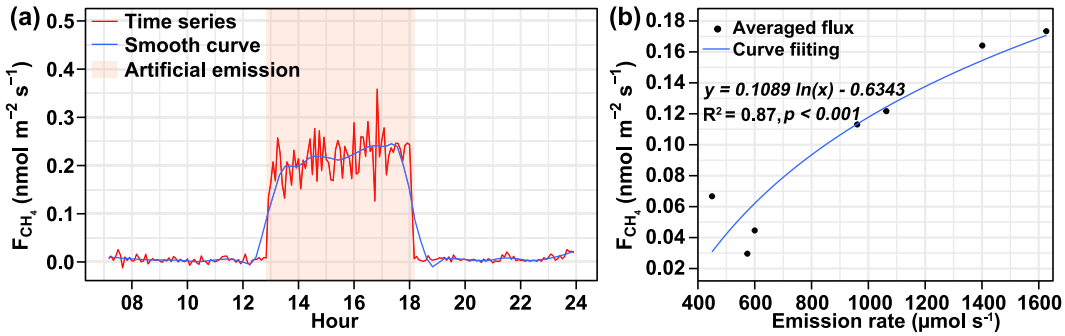

Figure 3. (a) The change of CH_4 flux during the artificial source emission experiment; (b) the average fluxes for different emission rates.

used 12 different periods, including 1, 2, 10, 15, 20, 30, 60, 120, 180, 240, and 720 min, to analyze the impact of averaging period on eddy fluxes observed at ChinaFLUX sites, which found that more flux changing signals could be captured via a shorter period. Therefore, the model might cause different results under the influence of the averaging period, the study of the averaging periods was also very important to the model application. Occasionally, the measured wind direction was outside the set wind direction range during the discharge period, resulting in a discontinuous exhaust. However, this was inevitable in artificial tracer experiments, which caused a non-stationarity CH_4 flux. Given that (a) the measurements were under high QC level, (b) the stationarity changes with different period, (c) more flux changing signals could be captured via a shorter period avoiding the removal of effective emissions, the stationarity of turbulence was not utilized as a data quality criterion (Sun et al., 2006).

To ensure high data quality, we further filtered out the abnormal data. The data under poor experimental conditions and during equipment adjustment (e.g., pressure regulation or a short pause), however, were discarded. The data relating to the first and the last 5 minutes of the experiment were also discarded considering the temporary instability of CH_4 release and the turbulence transport time. The measured fluxes were a combination of background and artificial emissions (Figure 3a). The background methane flux, around 0.01 nmol m^{-2} s^{-1}, was steady during the experiment. Figure 3b shows the averaged flux response at different emission rates. The positive correlation confirms that the CH_4 flux at each emission rate was adequately and effectively observed in this study.

2.4. Footprint Modeling

The measured vertical turbulent flux F_z (nmol m^{-2} s^{-1}) by EC system can be determined by the combination of the corresponding surface flux and the footprint weighting factor:

$$F_z = \sum_0^i \sum_0^j F_{ij}\phi_{ij}\Delta x_{ij}\Delta y_{ij} \quad (1)$$

where F_{ij} (nmol m^{-2} s^{-1}) is the surface flux density from cell ij, ϕ_{ij} (m^{-2}) is footprint function calculating the intensity of the sources contribution to measured flux from cell ij. Δx_{ij} (m) and Δy_{ij} (m) denotes x and y size of cell ij. The default cell size of the models is 1 × 1 m.

When only one cell is the source, the Equation 1 could be described as:

$$F_z = F_{ij,\text{source}}\phi_{ij,\text{source}}\Delta x_{ij,\text{source}}\Delta y_{ij,\text{source}} \quad (2)$$

where $F_{ij,\text{source}}$ (nmol m^{-2} s^{-1}) is the surface flux density from the single cell ij, $\phi_{ij,\text{source}}$ represents the cell's contribution intensity.

If we assume f_{source} to describe the whole source emission rate (nmol s^{-1}) from the cell, then $F_{ij,\text{source}}$ can be calculated as:

$$F_{ij,\text{source}} = f_{\text{source}} / (\Delta x_{ij,\text{source}}\Delta y_{ij,\text{source}}) \quad (3)$$

Finally, Equation 2 is simplified as:

$$F_z = f_{\text{source}}\phi_{\text{source}} \tag{4}$$

where ϕ_{source} (m^{-2}) is the source contribution intensity of the cell, that is, weight value calculated by footprint model.

Therefore, if flux contributions originate from two cells, that is, source_1 and source_2, we could obtain:

$$F_z = F_{\text{source1}}\phi_{\text{source1}}A_{\text{source1}} + F_{\text{source2}}\phi_{\text{source2}}A_{\text{source2}} \tag{5}$$

$$F_z = f_{\text{source1}}\phi_{\text{source1}} + f_{\text{source2}}\phi_{\text{source2}} \tag{6}$$

where F_{source1} and F_{source2} (nmol m^{-2} s^{-1}) denote the surface flux densities of the two cells. ϕ_{source1} and ϕ_{source2} (m^{-2}) are the contribution intensities, A_{source1} and A_{source2} (m^2) represent two cells' areas, f_{source1} and f_{source2} are the whole cell emission rates (nmol s^{-1}) of the two cells, respectively.

Based on the equations above, the emissions between LS release (f_{real}) and footprint model simulation ($f_{\text{estimated}}$) could be compared. The source emission rate (f_{source}), that is, estimated emission ($f_{\text{estimated}}$), could be calculated by F_z (measured by EC) and ϕ_{source} (calculated by footprint model). Further, because the source was artificially emitted, we knew and controlled the real emissions, that is, f_{real}. Finally, the differences between the model estimated emissions ($f_{\text{estimated}}$) and the real emissions (f_{real}) were compared under different experimental setups.

In our case, two categories of footprint models are used to calculate the contribution intensity of the LS, that is, ϕ_{source}. The first model is KM model (Kormann & Meixner, 2001), a fast analytical model based on boundary layer theory, and the other is called Flux Footprint Prediction (FFP) model (Kljun et al., 2015) parameterized and evaluated using simulations of the backward Lagrangian stochastic particle dispersion model LPDM-B (Wilson, 2015). In this study, the calculation of the KM model was developed based on the approach in EasyFlux-DL (Campbell Scientific Inc., 2017), and the FFP model was calculated using the approach by Kljun et al. (2015), available at http://footprint.kljun.net/index.php. FFP model is limited by stability, friction velocity, and measurement height, hence in practice, KM model is usually used instead of FFP model when the FFP model exceeds the limit range.

For KM model, input parameters are as follows:

- The measurement aerodynamic height (z_m), that is, z-d, the distance between measurement height (z) and zero-plane displacement height (d)
- The average wind speed at z_m ($\overline{U}$)
- The obukhov length (L)
- The standard deviation of lateral velocity fluctuations (σ_v)
- The friction velocity (u_*)
- The wind direction (WD), in cartesian coordinate system
- The cell size ($dx \times dy$), spatial resolution of footprint model

For FFP model, input parameters are as follows:

- The surface roughness length (z_0)
- The planetary boundary layer height (PBLH), computed by EasyFlux-DL (Campbell Scientific Inc., 2017)
- Other input parameters are same as KM model above

Flux footprint can be calculated by two models. In many cases, an aggregated footprint, a so-called footprint climatology, is of more interest to the user than a series of footprint estimates. All footprints for the time series are aggregated to a footprint climatology. The aggregated footprint can be normalized and presented for several levels of relative contribution to the total aggregated footprint (Kljun et al., 2015).

Table 1
The Input Physical Parameter of Two Footprint Models During the Experimental Period

Date	z_c (m)	d (m)	z_h (m)	z_e (m)	z_m (m)	z_0 (m)
2020-3-24	0.35	0.23	0.10	0	2.65	0.045
2020-4-09	0.45	0.30	0.10	0	2.55	0.068
2020-4-21	0.60	0.40	0.60	0.20	2.40	0.090
2020-4-26	0.60	0.40	0.60	0.20	2.40	0.100
2020-4-28	0.60	0.40	0.10	0	2.40	0.100

Note. z_c, canopy height; d, zero-plane displacement height; z_h, emission height; z_e, effective emission height; z_m, aerodynamic measuring height; z_0, surface roughness length.

Since the wind velocity was zero when the emission height (z_h) was lower than the zero-plane displacement height (d), the effective emission height (z_e) can, therefore, be calculated as:

$$z_e = \begin{cases} 0 & z_h < d \\ z_h - d & z_h > d \end{cases} \quad (7)$$

PBLH and z_0 are only required for FFP, where z_0 is a crucial parameter in quantifying momentum fluxes, which can affect the performance of FFP while PBLH has a negligible impact (Arriga et al., 2017; Dumortier et al., 2019; Heidbach et al., 2017). According to the wind profile under neutral conditions, z_0 is periodically updated as (Rosenberg et al., 1983):

$$z_0 = z \exp\left(-\frac{k\bar{u}}{u_*}\right) \quad (8)$$

where k is von Karman constant (0.41), $\bar{u}$ is mean horizontal wind speeds after tilt correction, and u_* is the friction velocity. All data are from the sonic anemometer measurements.

The Qt width (5 mm) was much lower than 1m, and the LS was simulated using 60 point-sources. Hence, it was hard to calculate the source area based only on the physical settings, that is, without the knowledge of the length and width of the LS. To resolve this issue, the "linewidth" (LW) was introduced. The LW was simulated but not actually existed, it means the width of the 60 point-sources. To calculate the source area, we need to know the length and width of the LS. The LS length was fixed at 60 m and we assumed that the source contribution intensity (source area) was uniform in each cell, hence the intensity of the LS contribution was determined by the width. According to Equations 3 and 4, we could obtain:

$$f_{source} = F_{source} A_{source} = F_{source} \times \text{line length}\,(60\ \text{m}) \times \text{LW} \quad (9)$$

where F_{source} (nmol m^{-2} s^{-1}) is the surface flux density measured by EC, f_{source} is the artificially source emission rates (nmol s^{-1}). When f_{source} (estimated emission) = f_{real} (real emission), the corresponding source width (i.e., LW) can be calculated, and it was the optimal line width.

3. Results and Discussion

3.1. The Effect of the Model Parameters

To evaluate the effect of different factors, that is, different emission heights, rates, distances, as well as different flux averaging periods, on the model performance, it was necessary to ensure that the original input parameters were the same, as listed in Table 1. This was to avoid introducing input parameter-related errors into the experimental configurations. To test the influence of z_0 on model estimation and derive the original optimal z_0 for the FFP, the piecewise z_0 based on its diurnal variation were used to fit the emissions (Figure 4). The results showed that z_0 could affect model estimation in this study since the estimated emission decreased with the increase of z_0, where the error reached 15%. Arriga et al. (2017) and Heidbach et al. (2017) proved the strong effect of z_0 on model outputs, which was consistent with this study.

LW was the right width of the 60 m point-sources line. In this case, different LW could affect the predicted emissions of models (Equation 4). Hence, we calculated the initial LW of the two models by fitting the averaged flux data and the fitting value with the real emission (Figure 5). It was observed that the estimation of both FFP and KM was significantly affected by the LW (Figure 5), that is, the ratio of $f_{estimated}/f_{real}$ decreased with the increase of

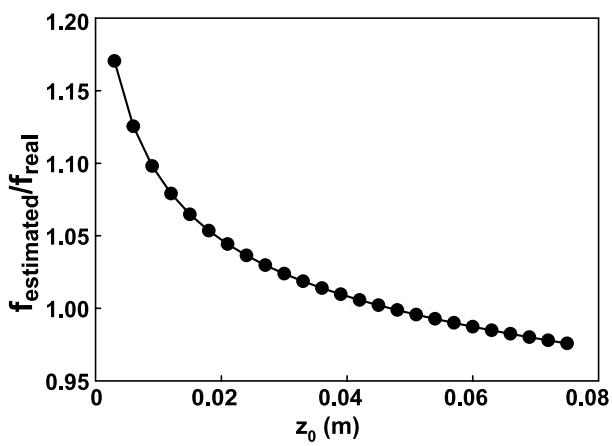

Figure 4. The influence of z_0 on the Flux Footprint Prediction model estimation. The estimated emission $f_{estimated}$ was normalized using the real emission f_{real}.

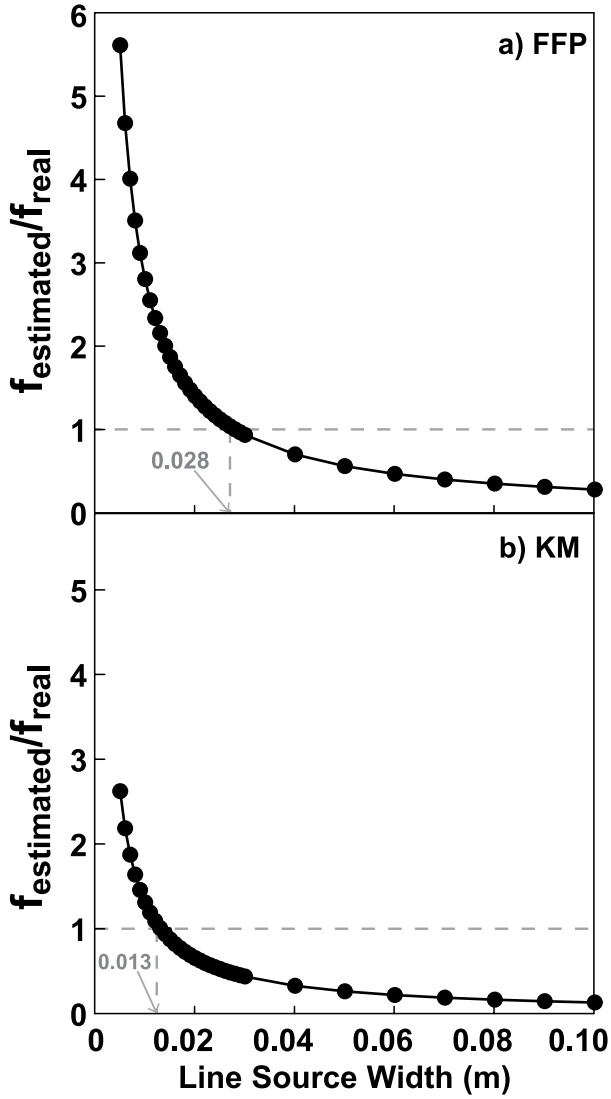

Figure 5. The effect of different line source widths on the model performance. The estimated emission $f_{estimated}$ was normalized using the real emission f_{real}.

Table 2
The Calculated Real Emission (μmol s^{-1}) According to Different Configurations

	SL			CL		
	5min	15 min	30 min	5min	15 min	30 min
LE	599.9	589.6	589.6	511.9	509.4	510.9
ME	1,063.5	1,080.9	1,080.9	960.8	954.8	954.8
HE	1,513.9	1,504.5	1,480.1	–	–	–

Note. SL, soil level; CL, canopy level; LE, low emission; ME, moderate emission; HE, high emission.

the LW. For example, in the FFP, when the LW increased from 2.8 to 4 cm, $f_{estimated}/f_{real}$ decreased at the same scale, that is, from 1 to 2.8/4. The error was respectively greater than 500% for the FFP and 200% for the KM when the LW ranged from 5 to 100 mm, which was much more serious compared to the impact of z_0 on the model estimation. Finally, the original LW input was determined as 1.3 and 2.8 cm for KM and FFP, respectively. The impact of different factors on the LW was also studied in this paper (see Sec. 3.3).

Different model resolutions, that is, 0.1, 0.5, 1, and 2 m cell size, were also analyzed to evaluate the impact of resolution on the model estimation. The results revealed that the estimated emission increased when the cell size got larger, and the estimation was likely to be remain stable when the cell size was smaller than 1m. For the KM model, the estimation of 2 m was only 0.006% larger than that of 1m. For the FFP model, it was only 0.009% larger. When a much better resolution was chosen, for example, less than 0.5 m, the calculation became more time-consuming. Furthermore, an underestimation occurred since the original LW was initialized with a resolution of 1m; hence, the LW needed to be adjusted further to obtain the optimal estimate. Consequently, based on the estimated results and the real emissions, we selected the input resolution as 1 × 1m.

After the parameter adjustment, the estimated emission rates based on KM and the FFP model were 1,072.8 ± 1.2 and 1,065.7 ± 1.2 μmol s^{-1}, respectively, which were only 0.8% and 0.2% higher than the real emission (1,063.5 μmol s^{-1}, Table 2, Figure S3 in Supporting Information S1). The results showed that both models performed well after parameter adjustment. That was followed by the model estimations of all experimental setups, which were calculated based on the above analysis. Then, we further filtered the estimated results through a significantly higher regression coefficient. To be specific, for the statistical test with the *P*-value of greater than 0.05, the estimations were considered unreliable to be used for the subsequent analysis.

3.2. Footprint Distribution

KM and FFP showed certain differences in terms of crosswind-integrated footprints (Figure 6). FFP produced a closer peak contribution distance (x_{max}) than that of KM. For FFP, a large ϕ_j appeared in close distance, which sharply decreased when away from the tower (Figure 6a). Given that the distance between the EC system and the intersection of prevailing wind direction and the LS is 45.3 m, the peak distance calculated by FFP greatly deviated from the real situation, which was obviously underestimated (Figure 6b). Rannik et al. (2000) and Kljun et al. (2003) revealed that Lagrangian simulation moves x_{max} closer to the EC system when considering the along-wind turbulent diffusion. Heidbach et al. (2017) also reported the closer x_{max} for FFP. Fortunately, this underestimation can be eliminated by adjusting the linewidth. For KM, peak distance was coincidentally about 35 m, near 43.5 m, which indicated that KM was likely to perform better in estimating ϕ_j. This might also be the reason why the linewidth of KM was closer to the diameter of the quantitative tube. Although the peak distance of KM showed higher "relative uncertainty" than that of FFP (Figure 6a), KM's estimation of the crosswind-integrated footprint was still more accurate according to the LS location. The differences in ϕ_j for three distances (dashed lines) were also more reasonable when KM is used. The study by Van de Boer et al. (2013) and Heidbach et al. (2017) revealed an overestimation of the peak distance by KM, which is slightly different from our results. Besides, the intensity of contribution, that is, ϕ_{source}, computed by FFP was about twice of KM (Figure

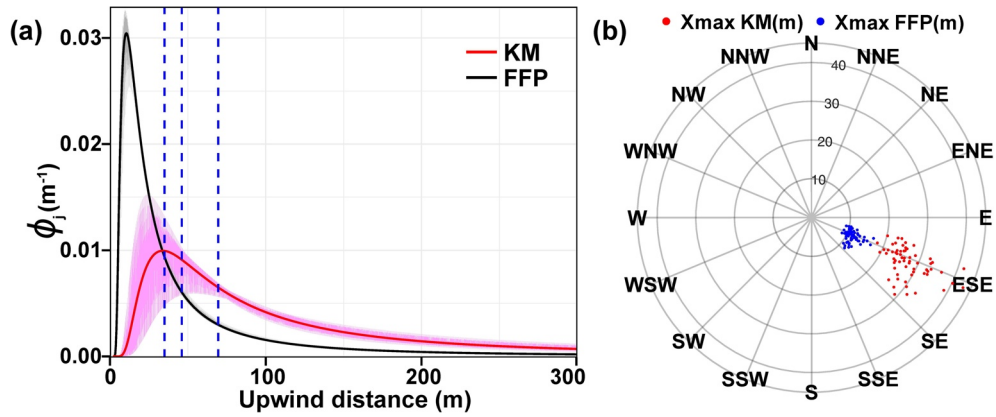

Figure 6. (a) The two-dimensional footprint density of the 124 crosswind integrated contributions (ϕ_j) calculated by Flux Footprint Prediction (FFP) and Kormann and Meixner (KM); (b) the wind-rose distribution of the peak contribution distance (x_{max}) by the two models. The bold lines show the average ϕ_j over along-wind distance. The shading in red (KM) and gray (FFP) are generated by the 124 overlapping curves of the crosswind-integrated footprint. The blue dotted lines indicate the closest distance (35 m), the intersection of prevailing wind direction and the line source (45.3 m), and the farthest distance (69.5 m).

S3 in Supporting Information S1) for adjusted LW (1.3 cm for KM and 2.8 cm for FFP). However, without LW adjustment, the integral area of curves between 35 and 69.5 m by KM was larger than that of FFP (Figure 6), which again indicated the significant influence of LW.

Figure 7 illustrates the 80% footprint climatology calculated by FFP and KM under different experiment setups. The KM produced a larger area of source contribution than the FFP for the same configurations. It is found that wind direction and velocity are the major factors affecting the models' area of source contributions. The fetch became longer with the higher wind velocity, and the bigger the span of wind direction, the wider the fetch (Figures 7 and S4 in Supporting Information S1). The footprint climatology and wind rose under LE, ME and HE configurations were performed for relatively low, high, and moderate wind velocities, respectively. Although LE corresponds to low wind velocity, the overall relationship between the emission rates and the wind velocities is not linear. The SL-ME configuration gives the highest wind velocity samples, the most concentrated wind direction and the least fetch deviation from the LS (Figures 7e and 7f and S4 in Supporting Information S1). The CL-ME, on the other hand, is with the lowest wind velocity samples, the relatively concentrated wind direction, and the less fetch deviation from the LS (Figures 7g and 7h). The 80% of source contribution regions estimated by KM could cover the entire LS, whereas the FFP cannot. Due to our physical setups, the inaccurate LS contribution estimated by FFP might be highly erroneous. The effective emission height difference between SL and CL is only 20 cm; hence, their influence on the footprint climatology might be submerged in the effect of wind direction and velocity (Zhang & Wen, 2015). In Section 3.5.4, we further assess the impact of different effective emission heights on the models. As a result, the footprint estimated by KM in this study is more robust since we consider the influence of both wind direction and the LS's coverage regions in our experiments.

3.3. Model Performance on Source Width

The influence of individual factors was important in the evaluation of the model application. Regardless of source type, that is, point or line, the actual source area was of utmost importance (Figure 5), which was determined by the LW. Although the individual factors alter the optimal LW, the consistency of LW was essential for good model estimation. Most experiments artificially set the source width to 1m to roughly match the default model resolution (1 × 1 m), which yield a bias in final estimation. However, up to now, there is still no work performing artificial tracer experiments to analyze the effect of source width. According to Equation 9, if the equipment supplying CH_4 did not change, and the F_{source} calculated by footprint model did not change, the linewidth should be a constant. Hence, in this study, we conducted different experiments to test model performance on LW.

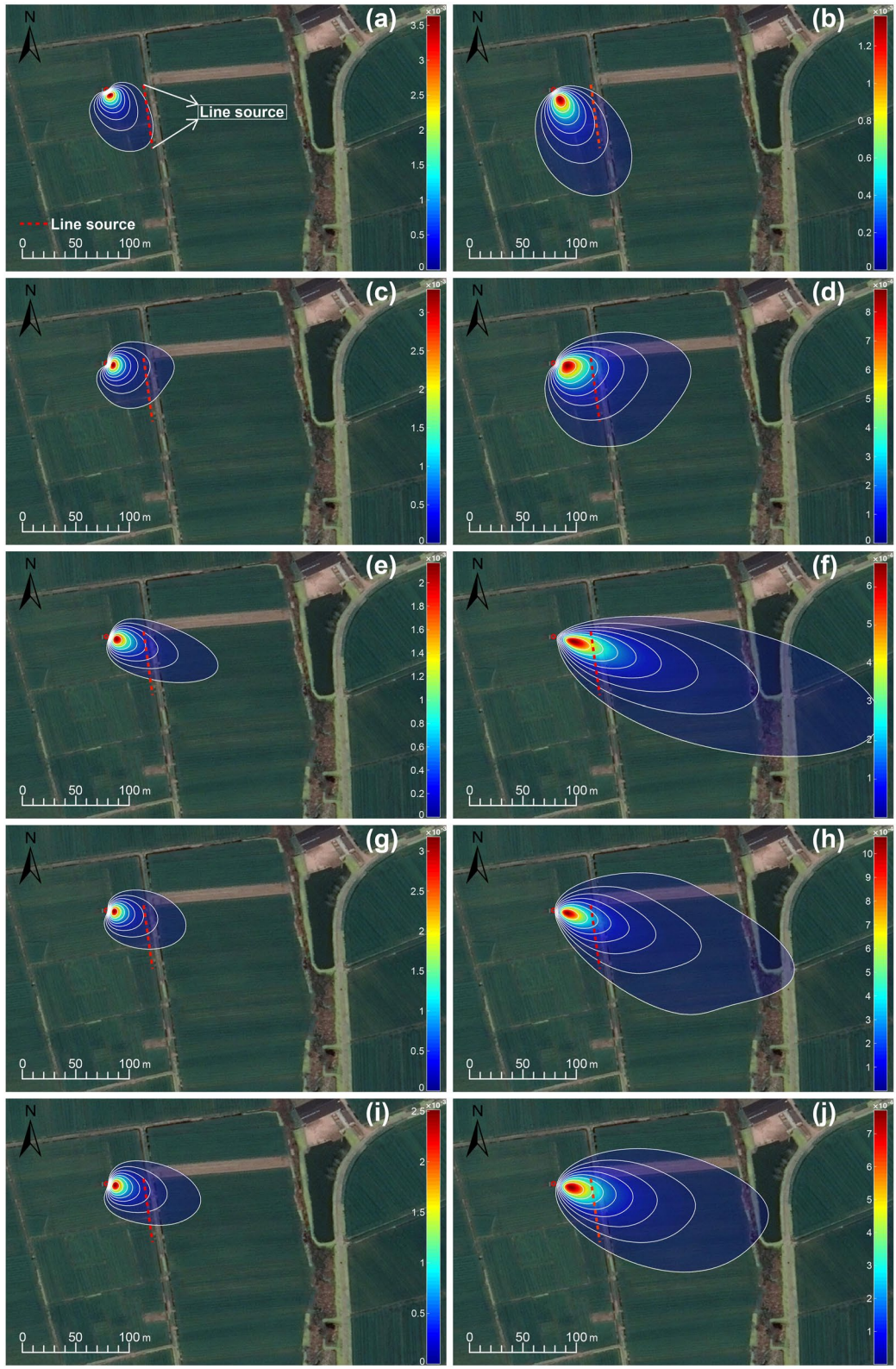

Figure 7. The contour lines (10%–80%) of the footprint climatology ϕ (m^{-2}) computed by Flux Footprint Prediction (a, c, e, g, i) and Kormann and Meixner (b, d, f, h, j). Different emission rates including low emission (a–d), moderate emission (e–h), and HE (i–j), and emission heights including soil level (a–b, e–f, i–j) and canopy level (c–d, g–h) are presented. The gradient colors indicate the source contribution strength. The red dashed lines indicate the line source. The remote sensing image layer was downloaded from © Google Earth.

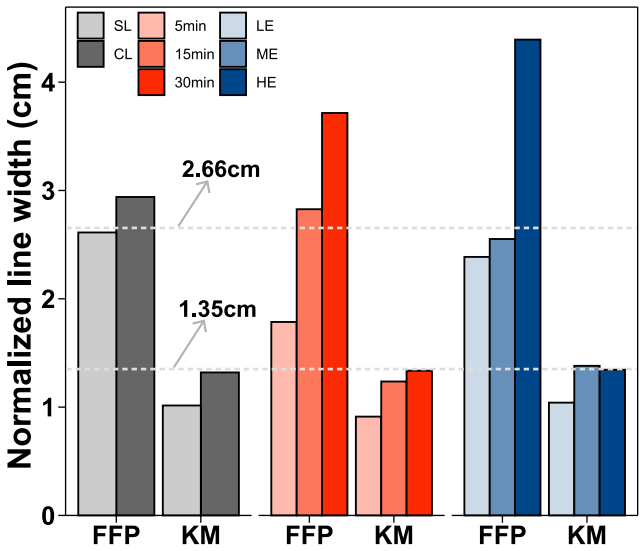

Figure 8. The influence of different individual factors, that is, footprint model, emission height, averaging period, and emission rate, on the linewidth. The normalized linewidth represents the adjusted linewidth in each configuration, that is, the corresponding linewidth when $f_{estimated}/f_{real} = 1$, to make different factors comparable. The dashed lines give the optimal combinations of the two models, where the average is 1.35 and 2.66 cm for Kormann and Meixner and Flux Footprint Prediction, respectively.

Figure 8 presents the normalized LW (for $f_{estimated}/f_{real} = 1$) under various individual factors, which can be easily determined by the equal-scaling relationship between LW (Figure 5) and the averaged normalized emission rate. All fitted emissions were filtered by P-value ($P < 0.05$) according to the filtered database. In theory, it is possible to procure 18 combinations, including the ones disregarded in the actual tests. Hence, to obtain the optimal combination of different setups, for example, SL-LE-5 min (each part delimited by dashes representing the factor level), the variations of 18 combinations were calculated for each model. If different factors returned with similar linewidth or minimum linewidth variations, the combination was recognized as the best, where the linewidth was accepted as reliable.

Hence, we considered the standard deviation as an evaluation indicator. The average standard deviation of the linewidth of different combinations was calculated as 0.16 by the KM model, and higher value was found for the FFP, that is, 0.58. This result indicated that the KM outperforms the FFP under complex measurement conditions. Besides, the LW of the FFP increased with the increase of emission height, averaging period, and the emission rate. The KM also showed an increasing LW trend, except for the HE rates with low sample sizes. Finally, for the KM, the CL-ME-30 min group achieved the best performance, with an average LW of 1.35 cm. For the FFP, the SL-ME-15 min was the best group with an average LW of 2.66 cm. Except for the inherent difference between the two models, similar to the source region distribution (Figure 7), whether the estimated source region can cover the entire LS might also be an important factor in model performance.

Based on the findings above, a multivariate regression model was proposed to predict the footprint model performance. The proposed model can be expressed for KM (Equation 10) and FFP (Equation 11) respectively as:

$$F_{sd} = -0.0017A_{interval} - 0.0007A_{height} + 0.15A_{emission} + 0.16 \quad (10)$$

$$F_{sd} = 0.003A_{interval} + 0.0002A_{height} + 1.85A_{emission} + 0.054 \quad (11)$$

where F_{sd} is the LW standard deviation of model estimation, A_{height} is the effective emission height of the source (cm), and $A_{interval}$ and $A_{emission}$ are the averaging period (min) and the emission rate (μmol s^{-1}) of the measured flux, respectively. In Equations 10 and 11, wind velocity is not considered as it is one of the input parameters of the models. When F_{sd} is the minimum, that is, its absolute value converges to zero, the model estimation can be assumed as the most accurate.

3.4. Overall Model Estimation

The estimated emissions using footprint models were normalized by the averaged LW of the optimal combination for FFP and KM models. Figure 9 presents all the normalized results. For these, the factor of source distance was analyzed based on all data (ALS, CLS, and LS), whereas the other factors were examined considering only the entire LS, that is, one level of the distance factor. That was to avoid introducing the error caused by the uniform linewidth for different distances into the analysis of other factors.

Overall, different configurations may greatly affect the footprint model performance. It can be seen that the majority of fitting results based on both models overestimated the emissions under CL, ME and HE configuration, where SL and LE returned the worst results in terms of underestimation (Figure 9). Similar to the result of the LW, the overestimation increased for long averaging periods (30 min) or with close source distance to the EC system (CLS). Combined with the footprint climatology results, the source contribution of SL and LE could not cover the entire line and the 80% source area by FFP was small (Figures 7a and 7c), hence the contribution on LS might not be accurate, too concentrated on the LS, finally leading to larger ϕ_{source} and lower estimation. In

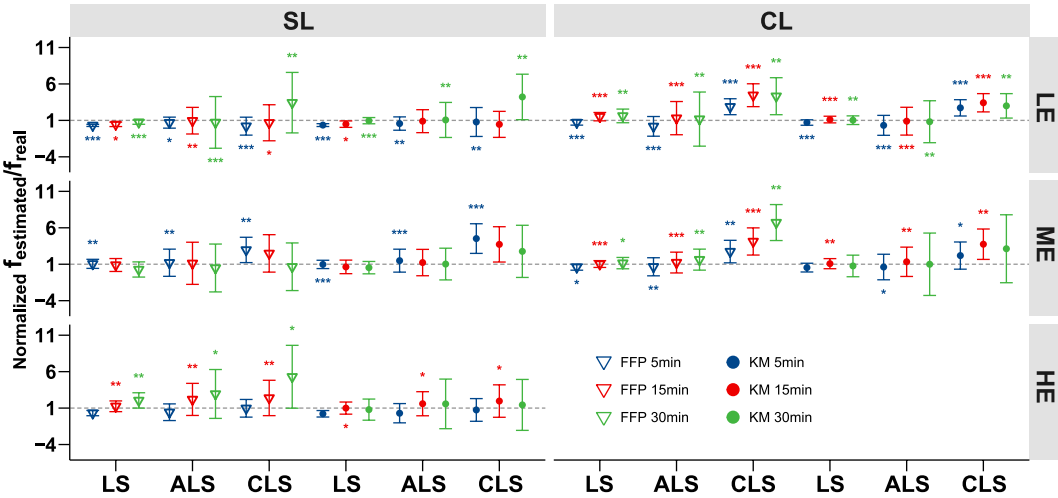

Figure 9. The normalized estimations of Flux Footprint Prediction (FFP) and Kormann and Meixner (KM) models. Different factors including emission height (soil level and canopy level), emission rate (low emission, moderate emission, and high emission), source distance (line source, ALS, and CLS), and averaging periods (5 min, 15 min, and 30 min), are presented. The $f_{estimated}$ was the optimal emission calculated by two models, which was initially normalized by the real emission (f_{real}), and then further normalized based on the optimal linewidth (1.35 cm for KM and 2.66 cm for FFP). The symbols *, **, and *** indicate significances at $P < 0.05$, $P < 0.01$, and $P < 0.001$, respectively. The error bars show 95% confidence intervals.

contrast, CL presented the larger source regions, and the high source contribution was too scattered (Figures 7d and 7h), which possibly resulted in lower ϕ_{source} and the model estimation might be stronger from the LS.

Since atmospheric stability was a key input parameter for both models and had an important influence on the footprint, we first evaluated its effect on model valuations before the analysis of different experimental configurations (Figure 10). With the change of atmospheric stability (z/L) from −0.1 to 0.1, both of the normalized footprint model results remained almost unchanged (Figure 10, the gray band shows the average) under the maximum samples (5 min). Moreover, KM model also performed well under 30 min interval, which shows the similar results in different atmospheric stability. However, FFP potentially overestimated the source emissions under unstable state in 15 and 30-min intervals (Figure 10, dotted oval). Thus, KM model may perform better under different atmospheric stability, the overall underestimation possibly can be explained by the inappropriate averaging period, which is analyzed and discussed in detail later.

3.5. Evaluation of Footprint Model Performance on Various Experimental Configurations

3.5.1. Footprint Model Performance on Source Distances

For the source distance, the estimation from the entire LS was slightly lower (~3.8%) than the real emission (Figure 11). Significant differences were observed between CLS and the other two estimations (LS and ALS). However, the difference between LS and ALS was not significant. When the emission source was close to the EC system (CLS), a high overestimation of 217.8% occurred, while ALS showed an overestimation of 12.2% for the real emission. The impact of source distance on model performance was similar to those of previous point-source studies, for example, Coates et al. (2017) and Heidbach et al. (2017). Dumortier et al. (2019) found that the distance has little impact on model estimation. Arriga et al. (2017) used a long tube as a linear source, placed at seven different places from the EC system at different times. They discovered that the normalized flux and the tube emission strength changed with distance. Furthermore, the shapes of the estimation curves, with a sharp growth for increasing distance toward a peak and a smooth decrease beyond, were similar to the shapes of the contribution intensity of the models.

When the LW was fixed, the overestimation of the maximum normalized flux would occur at the peak contribution distance. The sources located between the EC tower and the peak distance will be influenced by the distance more, and the emission valuation would fluctuate significantly. Hence, the LSs outside of the peak distance would be the best choice for experiments since the model valuation fluctuates the least with distance (Figure 6). In this

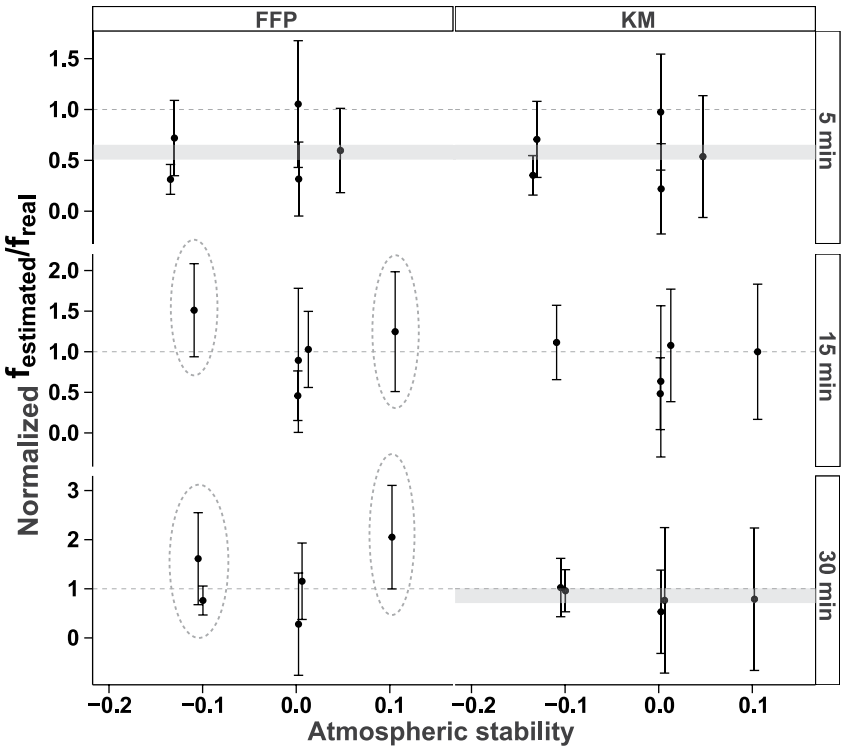

Figure 10. The influence of atmospheric stability on model estimation. The estimated emission $f_{estimated}/f_{real}$ was further normalized based on the optimal linewidth (1.35 cm for Kormann and Meixner and 2.66 cm for Flux Footprint Prediction) to make different factors comparable. The gray band gives the possible range of average estimation values under different stability. The error bars show 95% confidence intervals.

study, the LS was carried from 35 to 69.5 m, which was beyond the peak contribution distances of both models. The CLS (0–20 m) with overestimation was closer to the peak distance. LS and ALS (20–60 m), which had similar valuations, occupied more areas away from the peak distances. The crosswind-integrated curves showed the peak contribution closer to the CLS, especially for KM (Figure 6a), which may finally lead to the strong overestimation (Figure 11, CLS).

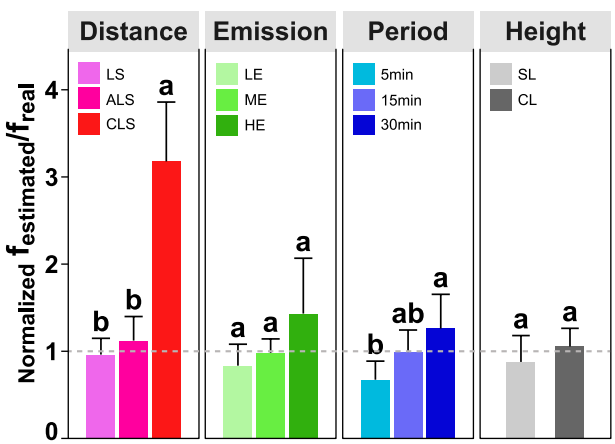

Figure 11. The influence of different levels of factors on model estimation. The estimated emission $f_{estimated}/f_{real}$ was further normalized based on the optimal linewidth (1.35 cm for Kormann and Meixner and 2.66 cm for Flux Footprint Prediction) to make different factors comparable. The normalization was performed separately based on different factors. Different letters indicate the significant differences between the cases in each factor (Turkey's HSD test, $P < 0.05$). The error bars show 95% confidence intervals.

3.5.2. Footprint Model Performance on Emission Rates

To the best of our knowledge, the effect of different emission rates on footprint models has not been studied before. For different emission rates (Figure 11), the estimated emissions increased for higher emissions, although no significant differences were found. The estimated emission calculated based on footprint model under LE showed an underestimation of 16.5%, and the best estimation was observed by ME, with only 1.9% lower than the real emission. However, a relatively large overestimation of 43.2% was made by HE. Especially at the SL, the estimated emission calculated based both models showed significant underestimation under LE despite the averaging period used. The averaging period, on the other hand, had opposite effects on the two models for the same emission rate, that is, ME-5 min or HE-15 min (Figure 9, LS). This suggested that the performance of footprint models (KM and FFP) might be mainly influenced by different emission rates at the SL. For the CL, the valuation of LE and ME showed a similar appearance when the same averaging period was used, that is, 5, 15 or 30 min for FFP and 15 min for KM (Figure 9, LS). This indicated the influence of the emission rate was insignificant at the CL for both models, and the averaging period plays a more important role.

3.5.3. Footprint Model Performance on Averaging Periods

Significant differences between the averaging periods of 5, 15, and 30 min were detected (Figure 11). The model estimation increased with the increase of the averaging period. In particular, the model achieved the highest estimation accuracy for the 15 min averaged flux, which was only 1% lower than the real emission. The biases for 5 and 30 min, however, were significantly larger and different, which denoted an underestimation of 32.6% and an overestimation of 26.1%, respectively. The poor performance of the footprint model was also observed for the 5 min averaging period. Equation 4 held under the hypothesis that the sources emit constantly. The time interval of the automatic discharging was set to 5 min by the control system (Section 2.2.3). A brief interruption could occur during the actual emissions if the wind direction exceeded the threshold. The emission source was volatile for the 5 min averaging period, which only got stable with the lengthening period. However, the periodic average was similar to a low-pass filter. The longer the period was, the more efficient the filter would be, eliminating the actual turbulence fluctuation. When the 15 and 30 min valuations in Figure 9 were observed, the influences of models are different, and the overestimation in 30 min was mostly contributed by the FFP model. For the KM model, the 30 min normalization is closer to one. This implied that the application of KM using a longer flux averaging period was better, while the FFP performed well with a moderate period. The study of Dumortier et al. (2019) demonstrated that the 15 min averaged data produced the best estimation, which was consistent with our predicted results by the FFP model.

3.5.4. Footprint Model Performance on Emission Heights

No studies have yet exactingly reported the model performance for different emission source heights. The experiment of CL and SL in this study returned an overestimation of 5.5% and an underestimation of 12.2%, respectively. The related studies, for instance, Dumortier et al. (2019) released the point sources at 0.8 m and revealed that the KM model performed well in an elevated emission height. However, the experiments were only conducted at one height. Arriga et al. (2017) used three different measurement heights to investigate model performance. Their results showed that the modeled footprint function, KM, was in a better agreement with the measurements at the lowest measurement point (0.7 m), which was equivalent to the highest emission height in our study, that is, CL. Furthermore, the footprint peak predicted by Lagrangian simulations presented a good agreement at a higher level (2.3 m), which was equivalent to the lowest emission height in our study, that is, SL (Figure 11).

When the emission height was far from the vegetation canopy, the turbulent exchange of source was little affected by the friction of the underlying surface, and hence the flux measured by EC system was more accurate. When the emission height was lower than the zero-plane displacement height, the turbulent exchange of source was greatly affected by the friction of underlying surface, eventually leading to an inadequate measurement and an underestimation at the SL. As seen in Figure 9, the normalized valuations of KM fluctuated around one at the CL, while all values were underestimated at the SL. Hence, the KM estimated the CH_4 sources better in CL compared to SL. The response of the FFP to the emission height was somewhat complex; the normalized valuations were fluctuating around one at both levels. Nevertheless, according to the optimal linewidth (Section 3.3), the best performance of FFP occurred at the SL, with an averaged normalized valuation of 0.98 and 1.10 at SL and CL, respectively. Therefore, the FFP estimated the CH_4 sources better in SL compared to CL. This result also verified the claims of Arriga et al. (2017). Additionally, we hold the opinion that the relatively small difference between the two emission heights had a certain degree of uncertainty, and thus the improved experiments with additional emission levels could achieve better validation.

4. Conclusions

The performance of footprint models was obviously changed under different experimental setups, including different emission heights, emission rates, and source distances. The parameters of roughness length (z_0) and linewidth (LW) could significantly affect the model estimation. It was of great significance to precisely adjust LW. When the source emission was at CL, the KM model showed good performance, while the FFP was better at the SL. The footprint model performance could be mainly influenced by different emission rates at the SL. In addition, for a longer averaging period, the KM was better, while FFP favored a moderate averaging period. The sources located between EC tower and peak contribution distance were more susceptible to the influence of distance, and thus the sources outside the peak distance were the best experimental choice for footprint model application. In addition, long-term experiments or experiments simulating gas emissions at different growth

stages of vegetation can offer more insights. A ring-like release experiment around the EC system or a multiple location experiment based on the LS system is also necessary to validate the performance of footprint models in specific ecosystems (e.g., grassland, sand land, and forest).

Conflict of Interest

The authors declare no conflicts of interest relevant to this study.

Data Availability Statement

The experimental data on the footprint model performance are openly available in jianguoyun repository at https://www.jianguoyun.com/p/DYEBdW4QsdbACBi2m8IEIAA.

Acknowledgments
This study was funded by the R&D Foundation of Jiangsu province, China (BK20220017) and the National Key Research and Development Program of China (2017YFC0209700).

References

Arriga, N., Rannik, U., Aubinet, M., Carrara, A., Vesala, T., & Papale, D. (2017). Experimental validation of footprint models for eddy covariance CO_2 flux measurements above grassland by means of natural and artificial tracers. *Agricultural and Forest Meteorology*, *242*, 75–84. https://doi.org/10.1016/j.agrformet.2017.04.006

Aubinet, M., Grelle, A., Ibrom, A., Rannik, U., Moncrieff, J., Foken, T., et al. (2000). Estimates of the annual net carbon and water exchange of forests: The Euroflux methodology. *Advances in Ecological Research*, *30*(30), 113–175.

Burba, G. G. (2001). Illustration of flux footprint estimates affected by measurement height, surface roughness and thermal stability. In K. Hubbards & M. Sivakumar (Eds.), *Automated weather stations for applications in agriculture and water resources management* (pp. 77–86).

Campbell Scientific Inc. (2017). EasyFlux DL CR3000OP for CR3000 and open-path eddy-covariance system, Instruction Manual (pp. G6–G7).

Chasmer, L., Kljun, N., Hopkinson, C., Brown, S., Milne, T., Giroux, K., et al. (2011). Characterizing vegetation structural and topographic characteristics sampled by eddy covariance within two mature aspen stands using lidar and a flux footprint model: Scaling to MODIS. *Journal of Geophysical Research*, *116*(G2), 19. https://doi.org/10.1029/2010jg001567

Coates, T. W., Flesch, T. K., McGinn, S. M., Charmley, E., & Chen, D. L. (2017). Evaluating an eddy covariance technique to estimate point-source emissions and its potential application to grazing cattle. *Agricultural and Forest Meteorology*, *234*, 164–171. https://doi.org/10.1016/j.agrformet.2016.12.026

Dumortier, P., Aubinet, M., Lebeau, F., Naiken, A., & Heinesch, B. (2019). Point source emission estimation using eddy covariance: Validation using an artificial source experiment. *Agricultural and Forest Meteorology*, *266*, 148–156. https://doi.org/10.1016/j.agrformet.2018.12.012

Finn, D., Lamb, B., Leclerc, M. Y., & Horst, T. W. (1996). Experimental evaluation of analytical and lagrangian surface-layer flux footprint models. *Boundary-Layer Meteorology*, *80*(3), 283–308. https://doi.org/10.1007/bf00119546

Flesch, T. K., Wilson, J. D., & Yee, E. (1995). Backward-time lagrangian stochastic dispersion models and their application to estimate gaseous emissions. *Journal of Applied Meteorology*, *34*(6), 1320–1332. https://doi.org/10.1175/1520-0450(1995)034<1320:btlsdm>2.0.co;2

Foken, T., Aubinet, M., & Leuning, R. (2012). The eddy covariance method. In M. Aubinet, T. Vesala, & D. Papale (Eds.), *Eddy covariance: A practical guide to measurement and data analysis* (pp. 1–19). Springer Atmospheric Sciences, Springer.

Foken, T., & Leclerc, M. Y. (2004). Methods and limitations in validation of footprint models. *Agricultural and Forest Meteorology*, *127*(3–4), 223–234. https://doi.org/10.1016/j.agrformet.2004.07.015

Gockede, M., Markkanen, T., Mauder, M., Arnold, K., Leps, J. P., & Foken, T. (2005). Validation of footprint models using natural tracer measurements from a field experiment. *Agricultural and Forest Meteorology*, *135*(1–4), 314–325. https://doi.org/10.1016/j.agrformet.2005.12.008

Gockede, M., Rebmann, C., & Foken, T. (2004). A combination of quality assessment tools for eddy covariance measurements with footprint modelling for the characterisation of complex sites. *Agricultural and Forest Meteorology*, *127*(3–4), 175–188. https://doi.org/10.1016/j.agrformet.2004.07.012

Heidbach, K., Schmid, H. P., & Mauder, M. (2017). Experimental evaluation of flux footprint models. *Agricultural and Forest Meteorology*, *246*, 142–153. https://doi.org/10.1016/j.agrformet.2017.06.008

Horst, T. W., & Lenschow, D. H. (2009). Attenuation of scalar fluxes measured with spatially-displaced sensors. *Boundary-Layer Meteorology*, *130*(2), 275–300. https://doi.org/10.1007/s10546-008-9348-0

Horst, T. W., & Weil, J. C. (1995). How far is far enough—The fetch requirements for micrometeorological measurement of surface fluxes (vol 11, pg 1018, 1994). *Journal of Atmospheric and Oceanic Technology*, *12*(2), 447. https://doi.org/10.1175/1520-0426(1995)012<0447:>2.0.co;2

Kaimal, J. C., Clifford, S. F., & Lataitis, R. J. (1989). Effect of finite sampling on atmospheric spectra. *Boundary-Layer Meteorology*, *7*, 827–837.

Kljun, N., Calanca, P., Rotach, M. W., & Schmid, H. P. (2015). A simple two-dimensional parameterisation for flux footprint prediction (FFP). *Geoscientific Model Development*, *8*(11), 3695–3713. https://doi.org/10.5194/gmd-8-3695-2015

Kljun, N., Kormann, R., Rotach, M. W., & Meixer, F. X. (2003). Comparison of the Langrangian footprint model LPDM-B with an analytical footprint model. *Boundary-Layer Meteorology*, *106*(2), 349–355. https://doi.org/10.1023/a:1021141223386

Kljun, N., Rotach, M. W., & Schmid, H. P. (2002). A three-dimensional backward lagrangian footprint model for a wide range of boundary-layer stratifications. *Boundary-Layer Meteorology*, *103*(2), 205–226. https://doi.org/10.1023/a:1014556300021

Kormann, R., & Meixner, F. X. (2001). An analytical footprint model for non-neutral stratification. *Boundary-Layer Meteorology*, *99*(2), 207–224. https://doi.org/10.1023/a:1018991015119

Leclerc, M. Y., & Foken, T. (2014). *Footprints in micrometeorology and ecology*. Springer-Verlag.

Leclerc, M. Y., Karipot, A., Prabha, T., Allwine, G., Lamb, B., & Gholz, H. L. (2003). Impact of non-local advection on flux footprints over a tall forest canopy: A tracer flux experiment. *Agricultural and Forest Meteorology*, *116*(3–4), 231. https://doi.org/10.1016/s0168-1923(03)00075-3

Leclerc, M. Y., Shen, S. H., & Lamb, B. (1997). Observations and large-eddy simulation modeling of footprints in the lower convective boundary layer. *Journal of Geophysical Research: Atmospheres*, *102*(D8), 9323–9334. https://doi.org/10.1029/96jd03984

Leclerc, M. Y., & Thurtell, G. W. (1990). Footprint prediction of scalar fluxes using a Markovian analysis. *Boundary-Layer Meteorology*, *52*(3), 247–258. https://doi.org/10.1007/bf00122089

Marcolla, B., & Cescatti, A. (2005). Experimental analysis of flux footprint for varying stability conditions in an alpine meadow. *Agricultural and Forest Meteorology*, *135*(1–4), 291–301. https://doi.org/10.1016/j.agrformet.2005.12.007

Mauder, M., & Foken, T. (2011). *Documentation and instruction manual of the eddy covariance software package TK3* (Vol. 46, pp. 1614–8924). Universität Bayreuth, Abteilung Mikrometeorologie, Arbeitsergebnisse.

McDermitt, D., Burba, G., Xu, L., Anderson, T., Komissarov, A., Riensche, B., et al. (2011). New low-power, open-path instrument for measuring methane flux by eddy covariance. *Applied Physics B*, *102*(2), 391–405. https://doi.org/10.1007/s00340-010-4307-0

Moncrieff, J. B., Massheder, J. M., de Bruin, H., Elbers, J. A., Friborg, T., Heusinkveld, B., et al. (1997). System to measure surface fluxes of momentum, sensible heat, water vapour and carbon dioxide. *Journal of Hydrology*, *188–189*, 589–611.

Moore, C. J. (1986). Frequency response corrections for eddy correlation systems. *Boundary-Layer Meteorology*, *37*(1–2), 17–35. https://doi.org/10.1007/bf00122754

Nicolini, G., Fratini, G., Avilov, V., Kurbatova, J. A., Vasenev, I., Valentini, R., et al. (2017). Performance of eddy-covariance measurements in fetch-limited applications. *Theoretical and Applied Climatology*, *127*(3–4), 829–840. https://doi.org/10.1007/s00704-015-1673-x

Rannik, U., Aubinet, M., Kurbanmuradov, O., Sabelfeld, K. K., Markkanen, T., Vesala, T., et al. (2000). Footprint analysis for measurements over a heterogeneous forest. *Boundary-Layer Meteorology*, *97*(1), 137–166. https://doi.org/10.1023/a:1002702810929

Rannik, U., Sogachev, A., Foken, T., Gockede, M., Kljun, N., Leclerc, M. Y., et al. (2012). Footprint analysis. In M. Aubinet, T. Vesala, & D. Papale (Eds.), *Eddy covariance: A practical guide to measurement and data analysis* (pp. 211–261). Springer Atmospheric Sciences, Springer.

Rebmann, C., Kolle, O., Heinesch, B., Queck, R., Ibrom, A., Aubinet, M., et al. (2012). Data acquisition and flux calculations. In M. Aubinet, T. Vesala, & D. Papale (Eds.), *Eddy covariance: A practical guide to measurement and data analysis* (pp. 59–83). Springer Atmospheric Sciences, Springer.

Reth, S., Gockede, M., & Falge, E. (2005). CO_2 efflux from agricultural soils in Eastern Germany—Comparison of a closed chamber system with eddy covariance measurements. *Theoretical and Applied Climatology*, *80*(2–4), 105–120. https://doi.org/10.1007/s00704-004-0094-z

Rosenberg, N. J., Blad, B. B., & Verma, S. B. (1983). *Microclimate: The biological environment* (2nd edn., p. 135). John Wiley & Son.

Schmid, H. P. (2002). Footprint modeling for vegetation atmosphere exchange studies: A review and perspective. *Agricultural and Forest Meteorology*, *113*(1–4), 159–183. https://doi.org/10.1016/s0168-1923(02)00107-7

Schotanus, P. S., Nieuwstadt, F. T. M., & Debruin, H. A. R. (1983). Temperature measurement with a sonic anemometer and its application to heat and moisture flux. *Boundary-Layer Meteorology*, *26*(1), 81–93. https://doi.org/10.1007/bf00164332

Schuepp, P. H., Leclerc, M. Y., Macpherson, J. I., & Desjardins, R. L. (1990). Footprint prediction of scalar fluxes from analytical solutions of the diffusion equation. *Boundary-Layer Meteorology*, *50*(1–4), 353–373. https://doi.org/10.1007/bf00120530

Steinfeld, G., Raasch, S., & Markkanen, T. (2008). Footprints in homogeneously and heterogeneously driven boundary layers derived from a lagrangian stochastic particle model embedded into large-eddy simulation. *Boundary-Layer Meteorology*, *129*(2), 225–248. https://doi.org/10.1007/s10546-008-9317-7

Sun, X. M., Zhu, Z. L., Wen, X. F., Yuan, G. F., & Yu, G. R. (2006). The impact of averaging period on eddy fluxes observed at ChinaFLUX sites. *Agricultural and Forest Meteorology*, *137*(3–4), 188–193. https://doi.org/10.1016/j.agrformet.2006.02.012

Tanner, C. B., & Thurtell, G. W. (1969). *Anemoclinometer measurements of Reynolds stress and heat transport in the atmospheric surface layer science lab* (pp. R1–R10). US Army Electronics Command, Atmospheric Sciences Laboratory TR ECOM 66-G22-F.

Van de Boer, A., Moene, A. F., Schuttemeyer, D., & Graf, A. (2013). Sensitivity and uncertainty of analytical footprint models according to a combined natural tracer and ensemble approach. *Agricultural and Forest Meteorology*, *169*, 1–11. https://doi.org/10.1016/j.agrformet.2012.09.016

Van Dijk, A. (2002). Extension of 3D of "the effect of linear averaging on scalar flux measurements with a sonic anemometer near the surface" by Kristensen and Fitzjarrald. *Journal of Atmospheric and Oceanic Technology*, *19*(1), 80–19. https://doi.org/10.1175/1520-0426(2002)019<0080:etoteo>2.0.co;2

Wagle, P., Gowda, P. H., Neel, J. P. S., Northup, B. K., & Zhou, Y. T. (2020). Integrating eddy fluxes and remote sensing products in a rotational grazing native tallgrass prairie pasture. *Science of the Total Environment*, *712*, 136407. https://doi.org/10.1016/j.scitotenv.2019.136407

Webb, E. K., Pearman, G. I., & Leuning, R. (1980). Correction of flux measurements for density effects due to heat and water transfer. *Quarterly Journal of the Royal Meteorological Society*, *106*(447), 85–100. https://doi.org/10.1002/qj.49710644707

Wilson, J. D. (2015). Computing the flux footprint. *Boundary-Layer Meteorology*, *156*, 1–14. https://doi.org/10.1007/s10546-015-0017-9

Zhang, H., & Wen, X. F. (2015). Flux footprint climatology estimated by three analytical models over a subtropical coniferous plantation in southeast China. *Journal of Meteorological Research*, *29*(4), 654–666. https://doi.org/10.1007/s13351-014-4090-7